catalysts

MDPI

Article

Aqueous Miscible Organic LDH Derived Ni-Based Catalysts for Efficient CO_2 Methanation

Ziling Wang [1], Liang Huang [1,*], Tomas Ramirez Reina [2], Angelos M. Efstathiou [3] and Qiang Wang [1,*]

1 College of Environmental Science and Engineering, Beijing Forestry University, 35 Qinghua East Road, Haidian District, Beijing 100083, China; wangzl9094@bjfu.edu.cn
2 Department of Chemical and Process Engineering, University of Surrey, Guildford GU2 7XH, UK; t.ramirezreina@surrey.ac.uk
3 Chemistry Department, Heterogeneous Catalysis Lab, University of Cyprus, 1 University Ave., University Campus, Nicosia 2109, Cyprus; efstath@ucy.ac.cy
* Correspondence: l_huang@bjfu.edu.cn (L.H.); qiangwang@bjfu.edu.cn (Q.W.); Tel.: +86-136-9913-0626 (Q.W.)

Received: 2 August 2020; Accepted: 8 October 2020; Published: 12 October 2020

Abstract: Converting CO_2 to methane via catalytic routes is an effective way to control the CO_2 content released in the atmosphere while producing value-added fuels and chemicals. In this study, the CO_2 methanation performance of highly dispersed Ni-based catalysts derived from aqueous miscible organic layered double hydroxides (AMO-LDHs) was investigated. The activity of the catalyst was found to be largely influenced by the chemical composition of Ni metal precursor and loading. A Ni-based catalyst derived from AMO-Ni_3Al_1-CO_3 LDH exhibited a maximum CO_2 conversion of 87.9% and 100% CH_4 selectivity ascribed to both the lamellar catalyst structure and the high Ni metal dispersion achieved. Moreover, due to the strong Ni metal–support interactions and abundant oxygen vacancy concentration developed, this catalyst also showed excellent resistance to carbon deposition and metal sintering. In particular, high stability was observed after 19 h in CO_2/H_2 reaction at 360 °C.

Keywords: AMO-LDH; layered double oxides; CO_2 hydrogenation; methane; Ni catalyst

1. Introduction

The concentration of CO_2 in the atmosphere has risen from 270 to 385 ppm in the past 200 years which has been causing serious problems such as the greenhouse effect, global climate change, and glaciers melting [1–3]. Regarding these environmental issues, three ways to reduce CO_2 content in the atmosphere have been suggested [4–7], namely CO_2 emission reduction, CO_2 capture and storage (CCS), and CO_2 conversion and utilization.

CO_2 is chemically stable and it needs to be activated in the presence of hydrogen in order to convert it to CH_4. Although CO_2 activation is an endothermic process, thus requiring energy input, it can usually be integrated with fuel production from renewable energy, making CO_2 conversion in the Power-to-Gas (PtG) process a very promising green technology [4,8,9]. Due to a series of technological issues of storage and transportation, renewable energy can hardly be a primary source of energy for the society [10].

CO_2 methanation appears to be one of the largely investigated scientific topics [11,12]. Herein, CO_2 is hydrogenated to methane at relatively high temperatures, ca. 300–400 °C, known as the Sabatier reaction, which is a very promising approach for the storage of renewable energy [6]. Based on the PtG

concept, electricity generated by renewable energy is then used to produce hydrogen by electrolysis. The thus formed hydrogen is then used to produce selectively CH_4 by the reaction with CO_2 [13–15].

$$CO_{2(g)} + 4\ H_{2(g)} \rightarrow CH_{4(g)} + 2\ H_2O_{(g)}\ (\Delta H^\circ = -165\ \text{kJ/mol}) \quad (1)$$

Presently, CO_2 activation catalysts are under extensive investigation. Commonly used catalysts are group VIII noble metal-based catalysts, such as Rh, Ru, etc [16,17]. Moreover, non-precious metal-based in the group VIII, like Ni, Co, and Fe can also be used [18,19]. Noble metal-based catalysts show the best methanation catalytic performance, but their high cost limits large-scale utilization [20,21]. Among all the non-precious metals, although Fe-based catalysts are preferable because of their very low cost, they suffer from problems of low catalytic activity, coking, and deactivation after long time-on-stream [22]. On the other hand, Ni-based catalysts are currently used in Sabatier reaction due to their high activity and low cost [23–25]. For Ni-based catalysts, γ-Al_2O_3 has been widely used as support for its large specific surface area (SSA), high-temperature thermal resistance, and good chemical stability [26,27]. Benefiting from these features, Ni/γ-Al_2O_3 composite is the most broadly used catalytic system for CO_2 methanation.

LDHs is a family of ionic lamellar solid compounds consisting of positively charged brucite-like layers and exchangeable interlayer anions [28,29]. Group VIII metal ions can be inserted into the LDH precursor and then be reduced to form catalytically active metal nanoparticles [30–32]. Thus, the LDHs derived materials can be tuned for the carbon dioxide methanation to fulfill the following requirements: high basicity that is crucial for CO_2 activation (adsorption strength and capacity), and appropriate nickel dispersion and reducibility, necessary for this redox process [33–35]. Liu et al. [36] demonstrated that the interaction between metal nanoparticles and support can be strengthened due to chemical bonding, thus improving the anti-coking and anti-sintering properties of the supported metal catalysts. In addition, a novel method called aqueous miscible organic (AMO) treatment was described in our previous work to increase the SSA and total pore volume of the LDHs materials [30]. In this method, the LDHs were synthesized by the conventional co-precipitation strategy, but the final wet slurry was washed with an AMO solvent. If organic solvents are completely miscible with water, they will then replace surface bound water, which can often lead to dispersion into thin nanosheets or exfoliation to even single layers [37,38]. AMO treatment gives a much-diminished driving force for aggregation to dense agglomerates of LDHs, while improving the SSA and surface basic site density of catalysts, and ultimately enhancing the catalytic activity.

Herein, we report the use of AMO-LDH as precursors for the preparation of solids suitable for the CO_2 methanation reaction. Ni-based CO_2 methanation catalysts derived from NiAl LDHs precursors have been prepared by co-precipitation and further treatment with the AMO method [30,39,40]. Precursors and catalysts were characterized by powder X-ray diffraction (XRD), scanning electron microscope (SEM), and surface texture. The impact of Ni loading (wt%) and the factors influencing the CO_2 conversion and CH_4 selectivity over these AMO-NiAl layered double oxides (LDOs) catalysts, as well as their stability during a long-term CO_2 methanation reaction were examined.

2. Results and Discussion

2.1. Influence of Interlayer Anions of AMO-Ni_3Al_1 LDHs on CO_2 Methanation

Figure 1 shows the powder XRD patterns of LDH precursors with different interlayer anions (NO_3^- and CO_3^{2-}) before and after reduction. LDH precursors present typical characteristic peaks at 11.7°, 22.8° and 35.1°, corresponding to the reflections of (003), (006) and (012) facets of the LDH crystal phase, respectively, indicating the successful synthesis of LDHs [41]. The peak intensity of Ni_3Al_1-CO_3 LDH is higher than that of Ni_3Al_1-NO_3 LDH, suggesting that CO_3^{2-} intercalated LDH is better crystallized than the NO_3^- intercalated one. The XRD patterns of reduced samples show two intensive peaks at 2θ = 44.4 and 51.8°, corresponding to the reflections of (111) and (200) facets of metallic Ni, and no diffraction peaks due to the NiO phase could be observed [42]. This result shows

that NiO is rather completely reduced into metallic Ni. However, if strong Ni support interactions prevail, NiO might not be completely reduced into metallic Ni since small NiO particles (<4 nm) cannot be detected by XRD. Moreover, the γ-Al_2O_3 phase was not detected, result that might be related to its very low crystallinity. According to literature reports [30], the Al_2O_3 phase derived from LDH precursors generally exists in an amorphous phase. In order to better understand the dispersion of Ni on the catalyst surface, the TEM image and EDX element mapping images of the reduced AMO-Ni_3Al-CO_3 LDH solid are shown in Figures 2 and 3, respectively. Black dots in the TEM image represent the Ni particles, where a mean diameter of ~10 nm was estimated. From Figure 3b, it can be observed that Ni is evenly dispersed in the sample. Overall, it can be concluded that highly dispersed Ni-based catalysts were successfully synthesized from Ni-Al LDH precursors.

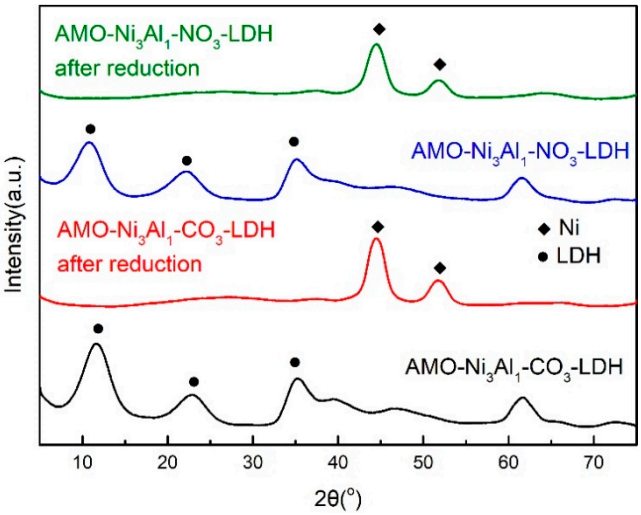

Figure 1. The powder XRD patterns of AMO-Ni_3Al-NO_3 LDH and AMO-Ni_3Al-CO_3 LDH precursors and their corresponding reduced samples.

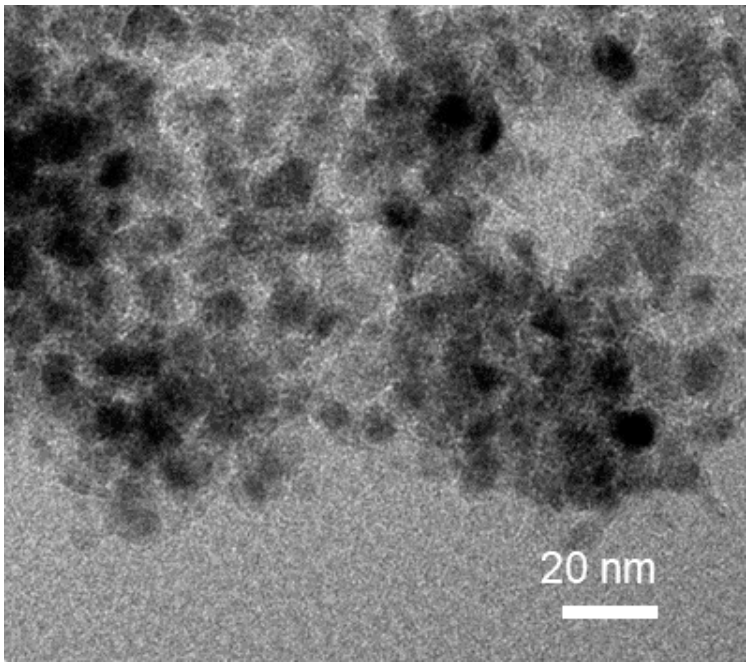

Figure 2. TEM image of reduced AMO-Ni_3Al-CO_3 LDH solid.

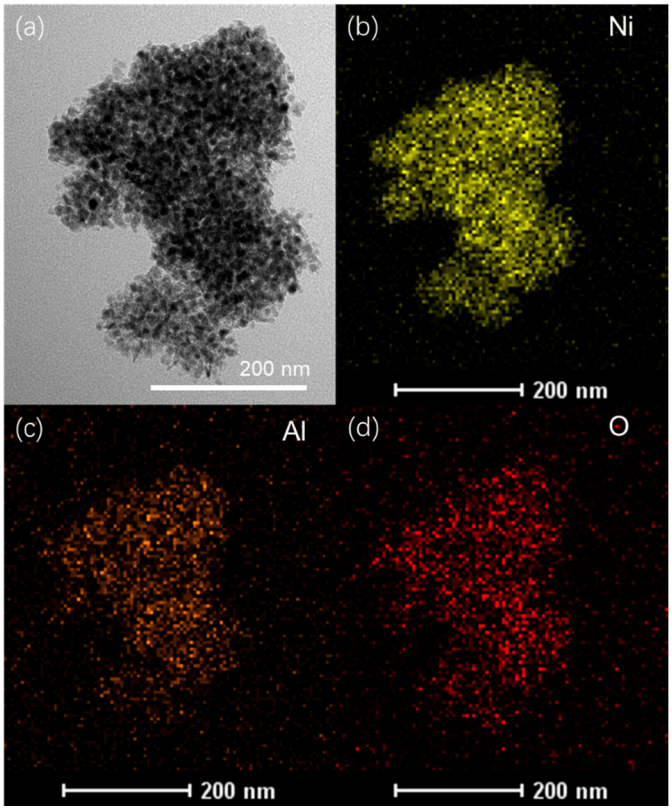

Figure 3. TEM image of reduced AMO-Ni_3Al-CO_3 LDH solid (**a**) and corresponding EDX elemental mapping of AMO-Ni_3Al-CO_3 LDH derived catalyst for Ni (**b**), Al (**c**), and O (**d**).

The CO_2 conversion and CH_4 selectivity over the AMO-Ni_3Al_1-CO_3-LDO and AMO-Ni_3Al_1-NO_3-LDO solids were compared and results are presented in Figure 4. These two catalysts show extremely high CH_4 selectivity, ca. 100% at T < 400 °C, although the conversion level is not remarkable in the low-temperature window, i.e., temperatures lower than 260 °C. Above 450 °C, the CH_4 selectivity starts to decrease, due to the competition with the reverse water-gas shift reaction (RWGS) which converts CO_2 to CO through hydrogenation ($CO_2 + H_2 \rightarrow CO + H_2O$) [43]. For both catalysts, the CO_2 conversion reaches maximum value at 360 °C, namely 87.9 and 84.2% over AMO-Ni_3Al_1-CO_3-LDO and AMO-Ni_3Al_1-NO_3-LDO, respectively. According to our previous study [44], interlayer anions influence the morphology and the interlayer distance of LDH, and the LDH with CO_3^{2-} interlayer has a larger SSA than the LDH with NO_3^- interlayer. The values of SSA of the pre-reduced catalysts, namely 158 m^2/g (AMO-Ni_3Al_1-CO_3-LDO) and 134 m^2/g (AMO-Ni_3Al_1-NO_3-LDO) are in good agreement with the previous study. Owing to the larger SSA, Ni produced after reduction will be likely better exposed, which might be one of the intrinsic reasons for the better activity performance of AMO-Ni_3Al_1-CO_3-LDO catalyst.

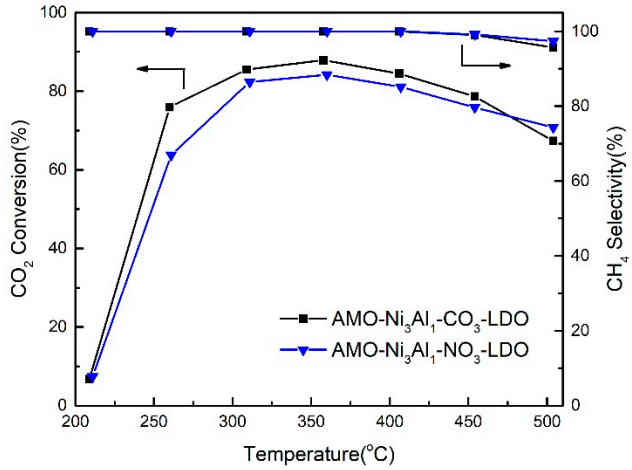

Figure 4. CO_2 conversion and CH_4 selectivity vs T profiles of AMO-Ni_3Al_1-CO_3-LDO and AMO-Ni_3Al_1-NO_3-LDO catalysts for the CO_2 methanation reaction.

2.2. *The Influence of Catalysts Preparation Procedure on the CO_2 Methanation*

The N_2 adsorption-desorption isotherms were measured for the as-synthesized carbonate intercalated LDHs derived catalysts, AMO-Ni_3Al_1-CO_3-LDO and C-Ni_3Al_1-CO_3-LDO, by coprecipitation and AMO treatment. These pre-reduced catalysts show different SSA, namely 117 m^2/g (C-Ni_3Al_1-CO_3-LDO) and 158 m^2/g (AMO-Ni_3Al_1-CO_3-LDO). AMO-Ni_3Al_1-CO_3-LDO, indicating that AMO treatment has a positive effect on increasing the SSA of LDH-derived solids. As previously reported [30,37], AMO treatment greatly reduces the driving force for aggregation to dense agglomerates, resulting in the increase of SSA.

The CO_2 methanation catalytic performance (CO_2-conversion and CH_4-selectivity) of AMO-Ni_3Al_1-CO_3-LDO and C-Ni_3Al_1-CO_3-LDO solids is illustrated in Figure 5. There is a significant difference in the CO_2-conversion (%) over the two catalysts between 250 and 350 °C. The optimal CO_2 conversion of AMO-Ni_3Al_1-CO_3-LDO is 88%, while that of C-Ni_3Al_1-CO_3-LDO is 82.5%. As discussed above, the AMO treatment is beneficial to increase the SSA of the solid, and this could lead to better Ni dispersion and thus to an increased CO_2 methanation activity per gram of solid basis.

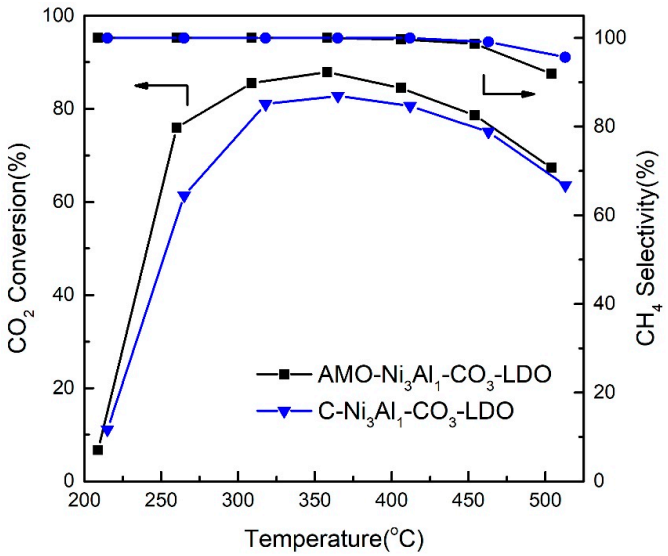

Figure 5. CO_2 conversion (%) and CH_4 selectivity (%) vs T profiles over AMO-Ni_3Al_1-CO_3-LDO and C-Ni_3Al_1-CO_3-LDO catalysts for the CO_2 methanation reaction.

2.3. Influence of Ni/Al Ratio on Catalyst CO_2 Methanation Activity

A series of NiAl-LDHs with different Ni/Al atom ratios were synthesized and their XRD patterns are shown in Figure 6. The X-ray diffraction peaks at 11.76, 22.84 and 35.2° prove that LDH precursors were successfully synthesized, and there are no obvious differences in the crystal structure of LDHs with different Ni/Al ratios. The precursors were then calcined and reduced (see Section 2.1) before CO_2 methanation activity tests. The CO_2 conversion (%) and CH_4 selectivity (%) vs temperature profiles obtained over these NiAl-LDHs catalysts are presented in Figure 7. AMO-Ni_2Al_1-CO_3-LDO presented the lowest CO_2 conversion among all the samples, especially at low temperatures. Upon increasing of the Ni/Al ratio to 3:1, the CO_2 conversion increase. As the Ni/Al ratio continues to increase to 4:1, the CO_2 conversion levels off, and becomes almost constant. This is likely because overloaded Ni can cause aggregation of Ni particles [45]. Hence, we identify a threshold for the positive impact of increasing Ni content on the catalytic CO_2 methanation activity being the Ni/Al ratio 4:1 the experimental limit to boost conversion. As for the selectivity to CH_4, by increasing the Ni/Al ratio no change is observed except a slight decrease at high temperatures (ca. 500 °C, Figure 7) due to the RWGS reaction.

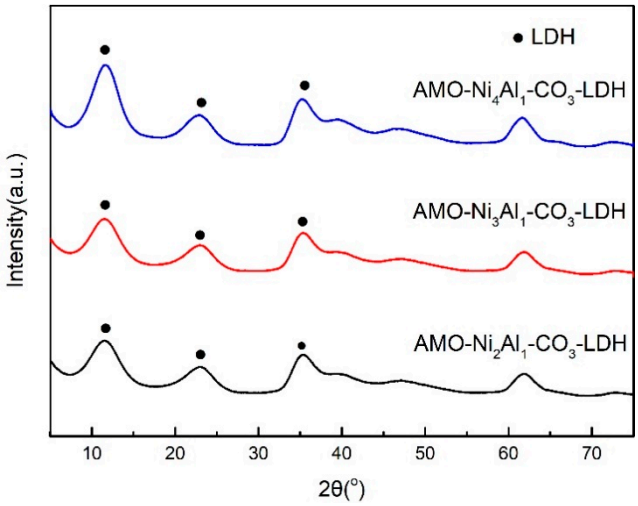

Figure 6. The powder XRD patterns of LDHs of different Ni/Al atom ratios (2:1, 3:1 and 4:1).

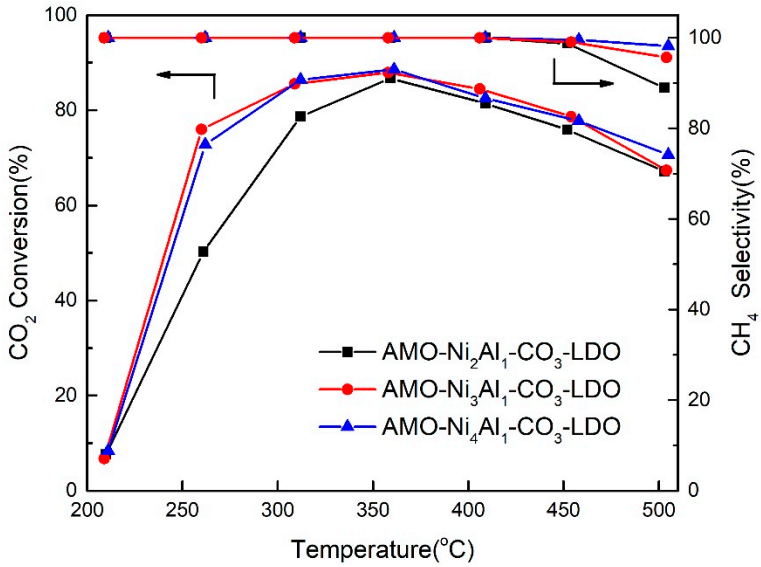

Figure 7. CO_2 conversion (%) and CH_4 selectivity (%) vs T profiles over AMO-Ni_2Al_1-CO_3-LDO, AMO-Ni_3Al_1-CO_3-LDO and AMO-Ni_4Al_1-CO_3-LDO catalysts for the CO_2 methanation.

2.4. Influence of Reduction Temperature in Hydrogen on Catalyst CO_2 Methanation Activity

Since the active component of the as-synthesized CO_2 methanation catalysts is the Ni metal, NiO (formed after calcination) should be reduced to metallic Ni (H_2 is used) before catalytic activity testing. The SEM images of AMO-Ni_3Al_1-CO_3 LDH, AMO-Ni_3Al_1-CO_3 LDO, and reduced AMO-Ni_3Al_1-CO_3 LDO solids are presented in Figure 8. Stacked and interlayered platelet-like crystals of LDH particles of a crystal particle size of ~60 nm are observed in Figure 8a, which is consistent with previous reports [46,47]. This typical platelet-like morphology remains after calcination. However, the morphology greatly changed after reduction in hydrogen.

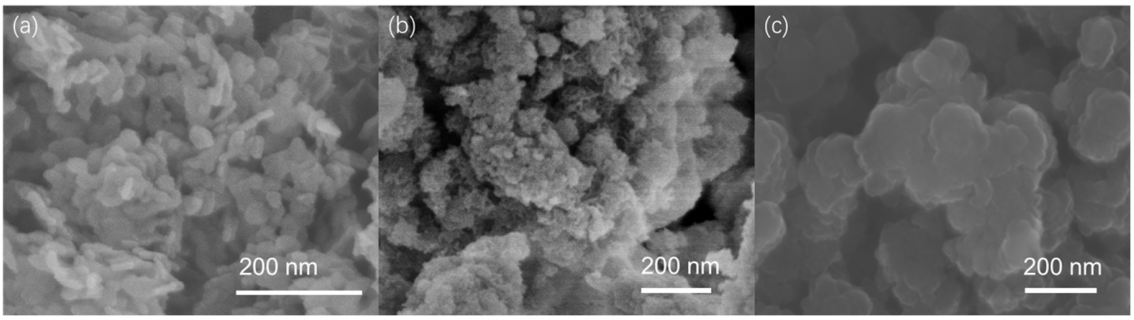

Figure 8. SEM images of AMO-Ni_3Al_1-CO_3 LDH (**a**), AMO-Ni_3Al_1-CO_3 LDO (**b**), and reduced AMO-Ni_3Al_1-CO_3 LDO (**c**) solids.

As shown in Figure 8c, spherical particles with a diameter of 100 ~ 200 nm are formed. The hydrogen treatment conditions had a great influence on the particle dispersion, morphology and structure, and these features would eventually affect the activity performance of the catalyst [30,48]. The powder XRD patterns of samples reduced at 500 and 600 °C are presented in Figure 9. After hydrogen treatment at 600 °C for 1 h, the sample shows relatively strong diffraction peaks at 44.48 and 51.67° corresponding to the Ni phase. The main diffraction peaks for the NiO phase (ca. 37.25 and 44.48°) were not detected, indicating that NiO has been fully reduced to Ni [49]. However, the sample exhibited relatively weak peaks of Ni phase and clear peaks of NiO phase after H_2 treatment at 500 °C.

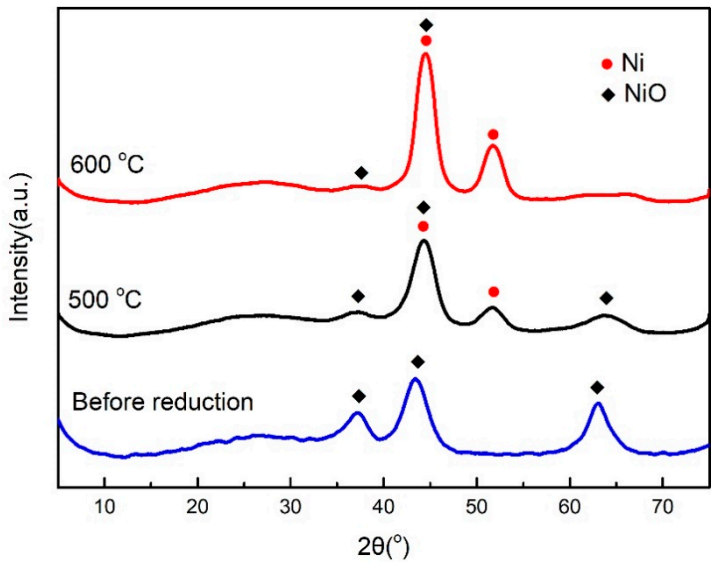

Figure 9. Powder XRD patterns of AMO-Ni_3Al_1-CO_3-LDO reduced in hydrogen at different temperatures, ca. 500 and 600 °C.

The H_2-TPR profile of the AMO-Ni_3Al_1-CO_3-LDO solid (Figure 10) shows its reducibility characteristics. It can be inferred that complete reduction of NiO cannot be accomplished at 500 °C, and it is envisaged that the full reduction temperature is at least 550 °C [50]. This is consistent with the powder XRD results that the sample reduced at 500 °C is not as complete as that reduced at 600 °C. It can be concluded that there exist strong metal–support interactions between NiO and Al_2O_3 surface [36,51–53].

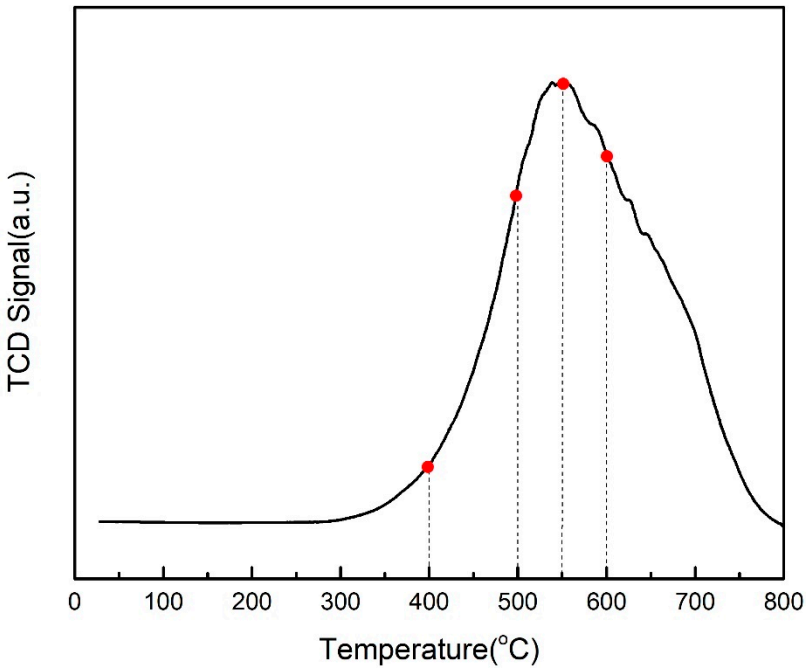

Figure 10. H_2-TPR profile of AMO-Ni_3Al_1-CO_3-LDO solid.

The effect of reduction temperature on the CO_2 conversion and CH_4 selectivity over the AMO-Ni_3Al_1-CO_3-LDO solid was investigated and results are presented in Figure 11. In all case, practically 100% CH_4-selectivity (no CO formation) was detected below 400 °C. The CO_2 conversion reaches its maximum value at 360 °C, namely 87.9%, 86.3%, 85.5%, and 77.5% for the catalysts reduced at 600, 550, 500, and 400 °C, respectively. A significant improvement of CO_2 conversion can be seen after increasing the hydrogen reduction temperature from 400 to 600 °C, especially for the CO_2 methanation reaction occurred at 260 °C. As discussed above, with the increase of reduction temperature, more NiO was converted into Ni, which leads to a high activity. Based on the results of powder XRD, H_2-TPR and catalytic tests, it can be stated that the degree of supported Ni reduction is influenced by the hydrogen reduction temperature and it has an important impact on the CO_2 conversion. It appears that 600 °C is the best reduction temperature for the present LDHs derived Ni-based CO_2 methanation catalysts. However, according to the H_2-TPR profile, the catalyst should be reduced completely at 550 °C. Since the H_2-TPR experiment is conducted dynamically, the reduction peak maximum may not appear at the exact temperature recorded. To ensure the thorough conversion of NiO into Ni, the hydrogen reduction temperature of the sample was set at 600 °C.

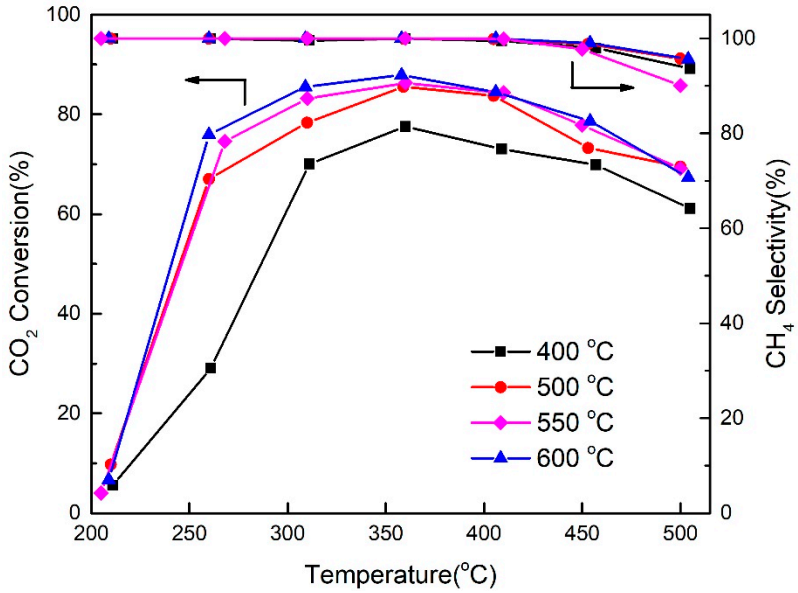

Figure 11. CO_2 conversion (%) and CH_4 selectivity (%) vs temperature profiles for the CO_2 methanation reaction over AMO-Ni_3Al_1-CO_3-LDO reduced in hydrogen at different temperatures, ca. 400, 500, 550 and 600 °C.

2.5. Stability Performance of AMO-Ni_3Al_1-CO_3-LDO

A stability test was performed on AMO-Ni_3Al_1-CO_3-LDO at 360 °C for 19 h and results are shown in Figure 12. Before any measurements, the catalyst was reduced at 600 °C for 1 h. The results obtained indicate that AMO-Ni_3Al_1-CO_3-LDO derived catalyst showed enhanced stability for long time-on-stream (TOS) since no obvious deactivation was observed (Figure 12). The CO_2 conversion remained above 87% and no CO was detected in the effluent gas stream. After the stability test, the spent catalyst was characterized by SEM. Figure 13 indicates the surface morphology of the spent catalyst. Compared with Figure 8c, the SEM images of spent catalysts show no obvious change in the particle configuration, which means that there were no structural changes in the solid catalyst. It was reported [22] that deactivation of CO_2 methanation catalysts is mainly caused by possible structural changes, such as sintering of the metal, and the generation of carbon deposits. By using AMO-Ni_3Al_1-CO_3 LDH as precursor, the obtained supported Ni nanoparticles exhibit a high degree of dispersion and strong metal–support interactions. Furthermore, the LDO support may provide oxygen vacancies [54], which are beneficial to the improvement of anti-sintering and anti-coking properties by providing an alternative route for CO_2 dissociation into CO and O (lattice oxygen), the latter being able to oxidize carbon (formed on Ni) formed by the reverse Boudouard reaction [55], so as to ensure its high activity during long-term operation.

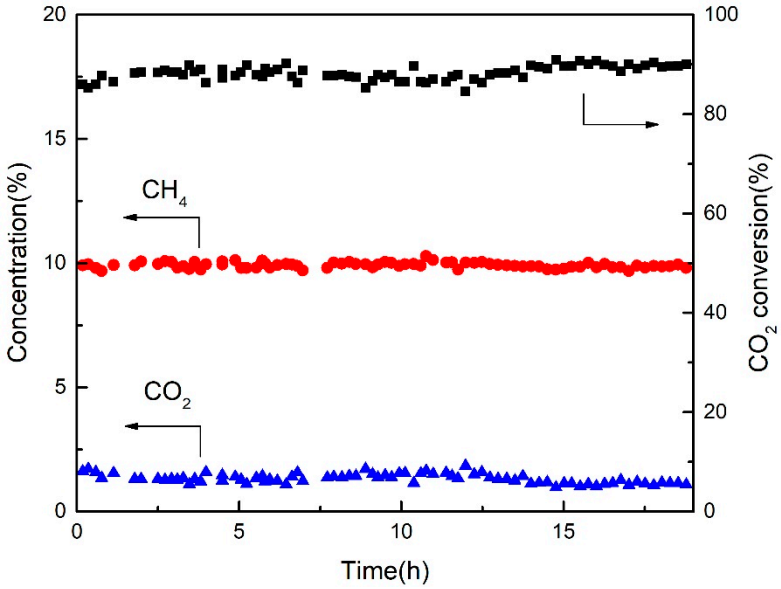

Figure 12. Stability performance of the AMO-Ni_3Al_1-CO_3-LDO catalyst at 360 °C in the CO_2 methanation reaction.

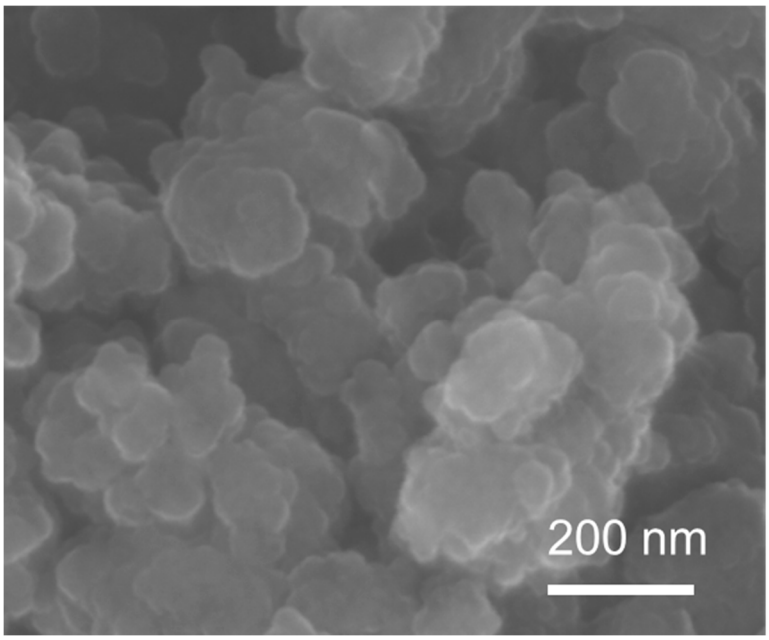

Figure 13. SEM images of used (19 h of CO_2 methanation) AMO-Ni_3Al_1-CO_3-LDO catalyst.

3. Experimental

3.1. Preparation of Catalysts

LDHs were first synthesized by the co-precipitation method. An aqueous solution containing nitrates of the metallic salts, ca. $Ni(NO_3)_2{\cdot}6H_2O$ and $Al(NO_3)_3{\cdot}9H_2O$ were added dropwise into a vigorously stirred Na_2CO_3 ($NaNO_3$ for NiAl-NO_3 LDH) solution. The pH of the resulting solution was kept constant at 10 by the addition of NaOH solution (4 M). The resulting slurry was stirred continuously for ~12 h at 30 °C, then filtered and washed several times with deionized water until pH reached 7, followed by drying at 60 °C in an oven. For AMO treatment, after the above-mentioned washing step, the resulting slurry was re-dispersed in ethanol for 2 h. The final solids were collected

by filtration and then dried at 60 °C for further characterization. To investigate the influence of Ni content, NiAl LDHs with different Ni/Al atom ratios (x = Ni/Al) were synthesized, which were denoted as Ni_xAl_1-LDH (x = 2, 3, and 4). The obtained LDHs were calcined at 400 °C for 5 h and reduced in 10 vol% H_2/Ar gas atmosphere (1 bar) before being used in any catalytic experiment.

3.2. Catalysts Characterization

Powder X-ray diffraction (PXRD) patterns of the solid AMO-NiAl LDOs samples were recorded using a Shimadzu XRD-7000 instrument in reflection mode and a Cu Kα radiation. The X-ray tube was operated at 40 kV and 40 mA while the accelerating voltage was set at 40 kV with 30 mA current (λ = 1.542 Å). Diffraction patterns were recorded within the range of 2θ = 5–75° with a scanning rate of 5°/min and a step size of 0.02°. Textural properties of the solids were analyzed using nitrogen adsorption-desorption isotherms obtained from a physisorption analyzer (SSA–7000, Builder, Beijing, China). SSA was estimated using the Brunauer−Emmett−Teller (BET) method. Before each measurement, ~0.1 g catalyst sample was degassed in a N_2/He gas mixture at 220 °C for 4 h.

Hydrogen temperature-programmed reduction (H_2-TPR) experiments were carried out in a multifunction chemisorption analyzer (PCA-1200, Builder, Beijing, China) equipped with a quartz U-tube reactor and a thermal conductivity detector (TCD) for gas analysis. For each test, a ~0.05 g sample was utilized. Before switching to the H_2/Ar gas stream, the sample was pretreated in Ar (40 mL/min) at 200 °C for 30 min and then cooled in Ar gas flow to 50 °C. The sample was then heated from 50 to 800 °C with a ramping rate of 10 °C/min in 5 vol% H_2/Ar gas mixture flow (30 mL/min). A field emission scanning electron microscope (SU-8010, Hitachi, Tokyo, Japan) was used to characterize the morphology of Ni33Al LDO (secondary agglomerated particles). A carbon tape was used to stick the powder to the SEM stage. Transmission electron microscopy (TEM) images were obtained on a FEI Tecnai G2 F30 (Hillsboro, USA) which was operated at 300 kV. Energy-dispersive X-ray (EDX) mapping characterizations of the composite oxides-based catalysts was made to investigate the distribution of the elements in the samples using the same TEM instrument.

3.3. Catalytic Activity Tests

The CO_2 methanation catalytic activity tests of the synthesized AMO-NiAl LDOs were carried out at 1 atm pressure in a fixed-bed stainless-steel micro-reactor. The stainless-steel micro-reactor was installed in a vertical split-tube furnace equipped with a proportional-integral-derivative (PID) temperature controller and several mass flow controllers. Before the catalytic performance test, a catalyst amount of W_{cat} = 0.1 g was first pretreated in 20 vol% H_2/N_2 gas mixture (50 mL/min) at 600 °C for 1 h, and then cooled to 200 °C in N_2 gas flow. Subsequently, a gas mixture of H_2, CO_2 and N_2 with a molar ratio of H_2/CO_2/Ar = 4:1:5 (ca. 40 vol% H_2/10 vol% CO_2/50 vol% Ar) was introduced into the reactor with a total flow rate of 80 mL/min corresponding to a space velocity of 48,000 mL $g_{cat}{}^{-1}$ h^{-1}. The methanation reaction was tested in the 200–500 °C range. After the reaction rate was stabilized at a given temperature after about 30 min, the composition of the effluent gas stream was analyzed online using a gas chromatography (SP-7890, Shandong Lunan, Zaozhuang, China) equipped with a TCD and FID detectors. The CO_2 conversion and CH_4 selectivity were estimated from the following Equations (2) and (3), respectively:

$$CO_2\ conversion(\%) = [\frac{[CO_{2,in}] - [CO_{2,out}]}{[CO_{2,in}]}] \times 100\% \quad (2)$$

$$CH_4\ selectivity(\%) = \frac{[CH_4]}{[CH_4] + [CO]} \times 100\% \quad (3)$$

In Equation (3), the *[CO]* concentration at the outlet of reactor refers to the non-selective CO_2 hydrogenation reaction towards CO and H_2O products (reverse water-gas shift reaction). Also, given the CO_2 feed composition used (10 vol%), the change in the outlet total molar flow rate of the

methanation reaction was small with respect to the inlet total molar flow rate, and this was considered in the estimation of CH_4 selectivity (Equation (3)).

4. Conclusions

Selective CO_2 methanation reaction was conducted over NiAl LDH derived catalysts which were prepared by coprecipitation and AMO treatment. AMO treated LDH exhibits higher SSA, which benefits Ni dispersion, than the conventional one. Highly dispersed Ni particles on the catalyst surface led to higher catalytic activity for CO_2 methanation. The Ni loading was found to play a key role in determining the catalytic activity by influencing the concentration of active sites along with the SSA. However, excessive Ni loading may result in Ni particle agglomeration, thus reducing the catalytic activity. As shown by the performed experiments, an optimal Ni/Al atom ratio of 3:1 was found. The catalyst reduction temperature by hydrogen was found to also play a role in its activity, which should be higher than 550 °C to ensure complete reduction of NiO to Ni. After hydrogen reduction at 600 °C, AMO-Ni_3Al_1-CO_3 LDH derived catalyst showed the highest CO_2 conversion (87.9%) and 100% CH_4 selectivity at 360 °C, due to the enhanced dispersion of Ni nanoparticles and SSA. Moreover, this AMO-Ni_3Al_1-CO_3 LDH derived catalyst shows remarkable stability in a 19-h activity test (above 87%) as the result of maintaining a highly dispersed Ni state, strong metal–support interactions, and abundant oxygen vacancy concentration.

Author Contributions: Conceptualization, L.H. and A.M.E.; Formal analysis, Z.W. and A.M.E.; Funding acquisition, Q.W.; Investigation, Z.W.; Methodology, Z.W. and L.H.; Project administration, Q.W.; Resources, T.R.R.; Supervision, Q.W.; Validation, L.H. and A.M.E.; Visualization, T.R.R.; Writing—original draft, Z.W.; Writing—review & editing, L.H., T.R.R., A.M.E. and Q.W. All authors have read and agreed to the published version of the manuscript.

Funding: This research was funded by the Fundamental Research Funds for the Central Universities (BLX201935, 2019JQ03015), the International Science and Technology Cooperation Project of Bingtuan (2018BC002), the Beijing Municipal Education Commission through the Innovative Transdisciplinary Program "Ecological Restoration Engineering", and International Science and Technology Cooperation Project of Bingtuan (No.2018BC002).

Conflicts of Interest: The authors declare no conflict of interest.

References

1. Mikkelsen, M.; Jørgensen, M.; Krebs, F.C. The teraton challenge. A review of fixation and transformation of carbon dioxide. *Energy Environ. Sci.* **2010**, *3*, 43–81. [CrossRef]
2. Smol, J.P. Climate Change: A planet in flux. *Nature* **2012**, *483*, S12–S15. [CrossRef] [PubMed]
3. Liang, S.; Altaf, N.; Huang, L.; Gao, Y.; Wang, Q. Electrolytic cell design for electrochemical CO_2 reduction. *J. CO_2 Util.* **2020**, *35*, 90–105. [CrossRef]
4. Li, W.; Nie, X.; Jiang, X.; Zhang, A.; Ding, F.; Liu, M. ZrO_2 Support Imparts Superior Activity and Stability of Co Catalysts for CO_2 Methanation. *Appl. Catal. B Environ.* **2018**, *220*, 397–408. [CrossRef]
5. Rahmani, S.; Rezaei, M.; Meshkani, F. Preparation of promoted nickel catalysts supported on mesoporous nanocrystalline gamma alumina for carbon dioxide methanation reaction. *J. Ind. Eng. Chem.* **2014**, *20*, 4176–4182. [CrossRef]
6. Renda, S.; Ricca, A.; Palma, V. Study of the effect of noble metal promotion in Ni-based catalyst for the Sabatier reaction. *Int. J. Hydrog. Energy* **2020**. [CrossRef]
7. Branco, J.B.; Brito, P.E.; Ferreira, A.C. Methanation of CO_2 over nickel-lanthanide bimetallic oxides supported on silica. *Chem. Eng. J.* **2020**, *380*, 122465. [CrossRef]
8. García-Gutiérrez, P.; Cuéllar-Franca, R.M.; Reed, D.; Dowson, G.; Styring, P.; Azapagic, A. Environmental sustainability of cellulosesupported solid ionic liquids for CO_2 capture. *Green Chem.* **2019**, *21*, 4100–4114. [CrossRef]
9. Zhou, Z.; Sun, N.; Wang, B.; Han, Z.; Cao, S.; Hu, D.; Zhu, T.; Shen, Q.; Wei, W. 2D-Layered Ni-MgO-Al_2O_3 Nanosheets for Integrated Capture and Methanation of CO_2. *ChemSusChem* **2019**, *13*, 360–368. [CrossRef]
10. Dou, L.; Yan, C.; Zhong, L.; Zhang, D.; Zhang, J.; Li, X.; Xiao, L. Enhancing CO_2 methanation over a metal foam structured catalyst by electric internal heating. *Chem. Commun.* **2020**, *56*, 205–208. [CrossRef]

11. Pastor-Pérez, L.; Patel, V.; Le Saché, E.; Reina, T.R. CO_2 methanation in the presence of methane: Catalysts design and effect of methane concentration in the reaction mixture. *J. Energy Inst.* **2020**, *93*, 415–424. [CrossRef]
12. Pastor-Pérez, L.; Saché, E.L.; Jones, C.; Gu, S.; Arellano-Garcia, H.; Reina, T.R. Synthetic natural gas production from CO_2 over Ni-x/CeO_2-ZrO_2 (x = Fe, Co) catalysts: Influence of promoters and space velocity. *Catal. Today* **2018**, *317*, 108–113. [CrossRef]
13. Jarvis, S.M.; Samsatli, S. Technologies and infrastructures underpinning future CO_2 value chains: A comprehensive review and comparative analysis. *Renew. Sustain. Energy Rev.* **2018**, *85*, 46–68. [CrossRef]
14. Thema, M.; Bauer, F.; Sterner, M. Power-to-Gas: Electrolysis and methanation status review. *Renew. Sustain. Energy Rev.* **2019**, *112*, 775–787. [CrossRef]
15. Dannesboe, C.; Hansen, J.B.; Johannsen, I. Catalytic methanation of CO_2 in biogas: Experimental results from a reactor at full scale. *React. Chem. Eng.* **2020**, *5*, 183–189. [CrossRef]
16. Beuls, A.; Swalus, C.; Jacquemin, M.; Heyen, G.; Karelovic, A.; Ruiz, P. Methanation of CO_2: Further insight into the mechanism over Rh/γ-Al_2O_3 catalyst. *Appl. Catal. B Environ.* **2012**, *113-114*, 2–10. [CrossRef]
17. Wang, F.; He, S.; Chen, H.; Wang, B.; Zheng, L.; Wei, M.; Evans, D.G.; Duan, X. Active Site Dependent Reaction Mechanism over Ru/CeO_2 Catalyst toward CO_2 Methanation. *J. Am. Chem. Soc.* **2016**, *138*, 6298–6305. [CrossRef]
18. Aziz, M.A.A.; Jalil, A.A.; Triwahyono, S.; Ahmad, A. CO_2 methanation over heterogeneous catalysts: Recent progress and future prospects. *Green Chem.* **2015**, *17*, 2647–2663. [CrossRef]
19. Sun, J.; Wang, Y.; Zou, H.; Guo, X.; Wang, Z.-J. Ni catalysts supported on nanosheet and nanoplate γ-Al_2O_3 for carbon dioxide methanation. *J. Energy Chem.* **2019**, *29*, 3–7. [CrossRef]
20. Ab Halim, A.Z.; Ali, R.; Wan Abu Bakar, W.A. CO_2/H_2 methanation over M*/Mn/Fe-Al_2O_3 (M*: Pd, Rh, and Ru) catalysts in natural gas; optimization by response surface methodology-central composite design. *Clean Technol. Environ. Policy* **2014**, *17*, 627–636. [CrossRef]
21. Zamani, A.H.; Ali, R.; Abu Bakar, W.A.W. Optimization of CO_2 methanation reaction over M*/Mn/Cu–Al_2O_3 (M*: Pd, Rh and Ru) catalysts. *J. Ind. Eng. Chem.* **2015**, *29*, 238–248. [CrossRef]
22. Lee, W.J.; Li, C.; Prajitno, H.; Yoo, J.; Patel, J.; Yang, Y.; Lim, S. Recent trend in thermal catalytic low temperature CO_2 methanation: A critical review. *Catal. Today* **2020**. [CrossRef]
23. Chein, R.-Y.; Wang, C.-C. Experimental Study on CO_2 Methanation over Ni/Al_2O_3, Ru/Al_2O_3, and Ru-Ni/Al_2O_3 Catalysts. *Catalysts* **2020**, *10*, 1112. [CrossRef]
24. Ghaib, K.; Ben-Fares, F.-Z. Power-to-Methane: A state-of-the-art review. *Renew. Sustain. Energy Rev.* **2018**, *81*, 433–446. [CrossRef]
25. Li, S.; Liu, G.; Zhang, S.; An, K.; Ma, Z.; Wang, L.; Liu, Y. Cerium-modified Ni-La_2O_3/ZrO_2 for CO_2 methanation. *J. Energy Chem.* **2020**, *43*, 155–164. [CrossRef]
26. Solis-Garcia, A.; Fierro-Gonzalez, J.C. Mechanistic Insights into the CO_2 Methanation Catalyzed by Supported Metals: A Review. *J. Nanosci. Nanotechnol.* **2019**, *19*, 3110–3123. [CrossRef] [PubMed]
27. Frontera, P.; Macario, A.; Monforte, G.; Bonura, G.; Ferraro, M.; Dispenza, G.; Antonucci, V.; Aricò, A.S.; Antonucci, P.L. The role of Gadolinia Doped Ceria support on the promotion of CO_2 methanation over Ni and Ni Fe catalysts. *Int. J. Hydrog. Energy* **2017**, *42*, 26828–26842. [CrossRef]
28. Wang, J.; Mei, X.; Huang, L.; Zheng, Q.; Qiao, Y.; Zang, K.; Mao, S.; Yang, R.; Zhang, Z.; Gao, Y.; et al. Synthesis of layered double hydroxides/graphene oxide nanocomposite as a novel high-temperature CO_2 adsorbent. *J. Energy Chem.* **2015**, *24*, 127–137. [CrossRef]
29. Huang, L.; Wang, J.; Gao, Y.; Qiao, Y.; Zheng, Q.; Guo, Z.; Zhao, Y.; O'Hare, D.; Wang, Q. Synthesis of $LiAl_2$-layered double hydroxides for CO_2 capture over a wide temperature range. *J. Mater. Chem. A* **2014**, *2*, 18454–18462. [CrossRef]
30. Wang, Q.; O'Hare, D. Large-scale synthesis of highly dispersed layered double hydroxide powders containing delaminated single layer nanosheets. *Chem. Commun.* **2013**, *49*, 6301. [CrossRef]
31. Climent, M.J.; Corma, A.; Iborra, S.; Epping, K.; Velty, A. Increasing the basicity and catalytic activity of hydrotalcites by different synthesis procedures. *J. Catal.* **2004**, *225*, 316–326. [CrossRef]
32. Gao, Y.; Zhao, Y.; Qiu, L.; Guo, Z.; O'Hare, D.; Wang, Q. Preparation of 4,4′-diaminostilbene-2,2′-disulfonic acid intercalated LDH/polypropylene nanocomposites with enhanced UV absorption property. *Polym. Compos.* **2017**, *38*, 1937–1947. [CrossRef]

33. Bian, L.; Wang, W.; Xia, R.; Li, Z. Ni-based catalyst derived from Ni/Al hydrotalcite-like compounds by the urea hydrolysis method for CO methanation. *RSC Adv.* **2016**, *6*, 677–686. [CrossRef]
34. Marocco, P.; Morosanu, E.A.; Giglio, E.; Ferrero, D.; Mebrahtu, C.; Lanzini, A.; Abate, S.; Bensaid, S.; Perathoner, S.; Santarelli, M.; et al. CO_2 methanation over Ni/Al hydrotalcite-derived catalyst: Experimental characterization and kinetic study. *Fuel* **2018**, *225*, 230–242. [CrossRef]
35. Abelló, S.; Berrueco, C.; Montané, D. High-loaded nickel-alumina catalyst for direct CO_2 hydrogenation into synthetic natural gas (SNG). *Fuel* **2013**, *113*, 598–609. [CrossRef]
36. Liu, J.; Bing, W.; Xue, X.; Wang, F.; Wang, B.; He, S.; Zhang, Y.; Wei, M. Alkaline-assisted Ni nanocatalysts with largely enhanced low-temperature activity toward CO_2 methanation. *Catal. Sci. Technol.* **2016**, *6*, 3976–3983. [CrossRef]
37. Chen, C.; Yang, M.; Wang, Q.; Buffet, J.-C.; O'Hare, D. Synthesis and characterisation of aqueous miscible organic-layered double hydroxides. *J. Mater. Chem. A* **2014**, *2*, 15102–15110. [CrossRef]
38. Ruengkajorn, K.; Erastova, V.; Buffet, J.-C.; Greenwell, H.C.; O'Hare, D. Aqueous immiscible layered double hydroxides: Synthesis, characterisation and molecular dynamics simulation. *Chem. Commun.* **2018**, *54*, 4394–4397. [CrossRef]
39. Chen, C.; Wangriya, A.; Buffet, J.-C.; O'Hare, D. Tuneable ultra high specific surface area Mg/Al-CO_3 layered double hydroxides. *Dalton Trans.* **2015**, *44*, 16392–16398. [CrossRef]
40. Cermelj, K.; Ruengkajorn, K.; Buffet, J.-C.; O'Hare, D. Layered double hydroxide nanosheets via solvothermal delamination. *J. Energy Chem.* **2019**, *35*, 88–94. [CrossRef]
41. Guo, X.; He, H.; Traitangwong, A.; Gong, M.; Meeyoo, V.; Li, P.; Li, C.; Peng, Z.; Zhang, S. Ceria imparts superior low temperature activity to nickel catalysts for CO_2 methanation. *Catal. Sci. Technol.* **2019**, *9*, 5636–5650. [CrossRef]
42. Yan, Y.; Dai, Y.; He, H.; Yu, Y.; Yang, Y. A novel W-doped Ni-Mg mixed oxide catalyst for CO_2 methanation. *Appl. Catal. B Environ.* **2016**, *196*, 108–116. [CrossRef]
43. Yang, L.; Pastor-Pérez, L.; Gu, S.; Sepúlveda-Escribano, A.; Reina, T.R. Highly efficient Ni/CeO_2-Al_2O_3 catalysts for CO_2 upgrading via reverse water-gas shift: Effect of selected transition metal promoters. *Appl. Catal. B Environ.* **2018**, *232*, 464–471. [CrossRef]
44. Wang, Q.; Wu, Z.; Tay, H.H.; Chen, L.; Liu, Y.; Chang, J.; Zhong, Z.; Luo, J.; Borgna, A. High temperature adsorption of CO_2 on Mg-Al hydrotalcite: Effect of the charge compensating anions and the synthesis pH. *Catal. Today* **2011**, *164*, 198–203. [CrossRef]
45. Zhen, W.; Li, B.; Lu, G.; Ma, J. Enhancing catalytic activity and stability for CO_2 methanation on Ni@MOF-5 via control of active species dispersion. *Chem. Commun.* **2015**, *51*, 1728–1731. [CrossRef]
46. Mak Yu, T.; Caroline Reis Meira, A.; Cristina Kreutz, J.; Effting, L.; Mello Giona, R.; Gervasoni, R.; Amado de Moura, A.; Maestá Bezerra, F.; Bail, A. Exploring the surface reactivity of the magnetic layered double hydroxide lithium-aluminum: An alternative material for sorption and catalytic purposes. *Appl. Surf. Sci.* **2019**, *467–468*, 1195–1203. [CrossRef]
47. Yan, Q.; Nie, Y.; Yang, R.; Cui, Y.; O'Hare, D.; Wang, Q. Highly dispersed Cu_yAlO_x mixed oxides as superior low-temperature alkali metal and SO_2 resistant NH_3 -SCR catalysts. *Appl. Catal. A Gen.* **2017**, *538*, 37–50. [CrossRef]
48. Wang, L.; Niu, X.; Chen, J. SiO_2 supported Ni-In intermetallic compounds: Efficient for selective hydrogenation of fatty acid methyl esters to fatty alcohols. *Appl. Catal. B Environ.* **2020**, *278*, 119293. [CrossRef]
49. Li, S.; Yang, Y.; Huang, S.; He, Z.; Li, C.; Li, D.; Ke, B.; Lai, C.; Peng, Q. Adsorption of humic acid from aqueous solution by magnetic Zn/Al calcined layered double hydroxides. *Appl. Clay Sci.* **2020**, *188*, 105414. [CrossRef]
50. Ye, R.-P.; Gong, W.; Sun, Z.; Sheng, Q.; Shi, X.; Wang, T.; Yao, Y.; Razink, J.J.; Lin, L.; Zhou, Z.; et al. Enhanced stability of Ni/SiO_2 catalyst for CO_2 methanation: Derived from nickel phyllosilicate with strong metal-support interactions. *Energy* **2019**, *188*, 116059. [CrossRef]
51. Xu, M.; He, S.; Chen, H.; Cui, G.; Zheng, L.; Wang, B.; Wei, M. TiO_{2-x}-Modified Ni Nanocatalyst with Tunable Metal–Support Interaction for Water–Gas Shift Reaction. *ACS Catal.* **2017**, *7*, 7600–7609. [CrossRef]
52. Mori, K.; Taga, T.; Yamashita, H. Isolated Single-Atomic Ru Catalyst Bound on a Layered Double Hydroxide for Hydrogenation of CO_2 to Formic Acid. *ACS Catal.* **2017**, *7*, 3147–3151. [CrossRef]

53. Zhang, J.; Wang, H.; Dalai, A. Development of stable bimetallic catalysts for carbon dioxide reforming of methane. *J. Catal.* **2007**, *249*, 300–310. [CrossRef]
54. Li, Z.; Yan, Q.; Jiang, Q.; Gao, Y.; Xue, T.; Li, R.; Liu, Y.; Wang, Q. Oxygen vacancy mediated Cu_yCo_3-yFe_1O_x mixed oxide as highly active and stable toluene oxidation catalyst by multiple phase interfaces formation and metal doping effect. *Appl. Catal. B Environ.* **2020**, *269*, 118827. [CrossRef]
55. Damaskinos, C.M.; Vasiliades, M.A.; Efstathiou, A.M. The effect of Ti^{4+} dopant in the 5 wt% $Ni/Ce_{1-x}Ti_xO_{2-\delta}$ catalyst on the carbon pathways of dry reforming of methane studied by various transient and isotopic techniques. *Appl. Catal. A Gen.* **2019**, *579*, 116–129. [CrossRef]